Theoretical Investigation of the Hydrogen Abstraction Reaction of the OH Radical with CH_2FCH_2F (HFC-152): A Dual-Level Direct Dynamics Study

Mahdi Taghikhani and G. A. Parsafar*

Department of Chemistry, Sharif University of Technology, Tehran 11365-9516, Iran

Received: March 27, 2007; In Final Form: June 16, 2007

The hydrogen abstraction reaction of the OH radical with CH_2FCH_2F (HFC-152) is studied theoretically over the 150−3000 K temperature range. In this study, the two most recently developed hybrid density functional theories, namely, BB1K and MPWB1K, are applied, and their efficiency in reaction dynamics calculation is discussed. The BB1K/6-31+G(d,p) method gives the best result for the potential energy surface (PES) calculations, including barrier heights, reaction path information (the first and second derivatives of PES), geometry of transition state structures, and even weak hydrogen bond orientations. The rate constants were obtained by the dual-level direct dynamics with the interpolated single-point energy method (VTST−ISPE) using the BB1K/MG3S//BB1K/6-31+G(d,p) quantum model. The canonical variational transition state theory (CVT) with the small-curvature tunneling correction methods are used to calculate the rate constants in comparison to the experimental data. The total rate constant and its temperature dependency in the form of a fitted three-parameter Arrhenius expression is $k(T) = 5.4 \times 10^{-13}(T/298)^{3.13} \exp\{-322/T\}$ cm^3 molecule^{-1} s^{-1}. A significant variational effect, which is not common generally for hydrogen-transfer reactions, is reported and analyzed.

I. Introduction

In the recent years, many groups have studied the role of the haloalkanes in the atmosphere.[1−4] The hydrofluorocarbons (HFCs) are a class of chemical substance that is introduced as ozone friendly alternatives for many industrial usages, such as foam blowing and refrigerants, because these materials do not take part in the ozone depletion process, unlike the chlorofluorocarbons (CFCs) and hydrochloroflourocarbons (HCFCs). In contrast, the HFCs have an important green house effect as the result of their high absorption of radiation in the infrared region. Therefore, experimental and theoretical kinetic studies of the HFCs have attracted considerable attention in the past decade. In order to determine the stability of a HFC species in the troposphere for use in kinetic modeling, its lifetime, rate constants, along with its temperature dependency, in reaction with various radicals must be calculated for atmospheric and combustion reactions.

HFC-152a and HFC-152 are widely used HFC compounds in industry. In our previous work,[5] we studied theoretically the reaction of OH and CH_3CHF_2 (HFC-152a). The CHF_2 position of the molecule was determined as a highly reactive site to form dominant channels at both thermodynamic and kinetic control conditions. We also reported quantum effects as a dominant nonclassical reflection effects for this reaction.

In this study, we have theoretically investigated kinetics of the hydrogen abstraction reaction from CH_2FCH_2F (HFC-152) with OH, as the most important radical species in atmospheric and combustion chemistry. Although the rate constant of the reaction of HFC-152 with OH has been measured by different groups experimentally, theoretical study only was done by Chandra et al. in 2000.[6] They applied QCISD(T)/6-311G(d,p)//MP2/6-311G(d,p) and PMP2=full/6-311G(3d,2p)//MP2/6-311G(d,p) quantum models. For dynamics modeling, they used transition state theory with crude tunneling correction methods of Eckart and Winger, in which they used imaginary frequency to estimate curvature of the reaction path, to evaluate the rate constant in comparison to the only available experimental data of that time at 298 K. Their study led to a crude estimation of the rate constant over the temperature range of 280−650 K such that only from their study the importance of the tunneling effect can be understood. In 1995, the reaction was studied by Kwok and Atkinson to measure the rate constant for a wide variety of compounds with an estimation method at 298 K.[7] Another experimental study in 1995 was carried out by Hsu and DeMore[8] with a relative rate measurement technique in which the total rate constant was measured by detecting the ratio of HFC-152 concentration over ethane concentration. Recently in 2003, Kozlov et al.[9] measured the absolute total rate constant of the reaction over a rather wide temperature range, 210−480 K, and reported a small nonlinearity in a low-temperature limit, near 210 K. In their study, they emphasized on the inconsistency for temperature dependency of the rate constant, which had already been reported by the relative measurement techniques in the previous works. They introduced a new temperature dependency for the rate constant, based on their rather wide range of temperature by the absolute measurement techniques which they used. Moreover, Wilson and co-workers recently studied the reaction experimentally with an emphasis on group effects at 298 K.[10]

We have theoretically studied the reaction between CH_2FCH_2F and OH over the 150−3000 K temperature range. Vigorous quantum and dynamics models are applied in the calculation of the rate constant and its temperature dependency over the wide temperature range, which includes both atmospheric and combustion conditions. Here, we have revealed more details about the mechanism including different reactive channels, their properties, and degeneracies. A significant variational

* Corresponding author. E-mail: Parsafar@sharif.edu. Tel.: + 98-21-66165355. Fax: + 98-21-66005718.

10.1021/jp072403s CCC: $37.00
Published on Web 07/28/2007

effect, which is not common in the hydrogen-transfer reactions, is also reported and analyzed. We have analyzed the spin contamination and basis set superposition errors (BSSE) to accentuate progressive aspects of the newly developed DFT methods in dynamics calculations.

II. Computational Methods

II.A. Electronic Structure Calculations. Recently, the efficient hybrid density functional theory (HDFT) methods were proposed as an alternative approach to the pure density functionals.[12] Recent HDFT methods introduce some additional kinetic energy density terms into exchange-correlation functionals[11] which play a significant role in the accuracy of the energy and geometry predictions for loose structures such as transition states (TS) and also in the modeling of weak interactions such as hydrogen bond or dispersion interaction of the van der Waals molecules.[11] The new functionals are named metafunctionals, and the resulting methods are called hybrid metadensity functional theory (HMDFT). In this study two MPWB1K[13] and BB1K[14] newly developed MHDFT methods are applied in comparison to the commonly used B3LYP and MP2 methods. The BB1K method of Zhao et al.[14] is a hybrid version of the BB95 density functional that mixes the Becke 1988 gradient-corrected exchange[15] and the 1995 kinetic-energy-dependent correlation[16] functionals with the fraction of HF exchange optimized for the prediction of thermochemical kinetics against a dataset of reaction energies and forward and reverse energy barriers.[17] BB1K was asserted to be the most powerful and accurate HMDFT method in the potential energy surface (PES) calculation of reactions.[14] This method was tested in comparison to the well-known MP2, MP3 MP4SDQ, QCISD, and QCISD(T) methods. The results show that this HMDFT method has a mean error which is several times smaller than those of MP2, MP3, MP4SDQ, and QCISD methods in the barrier height calculations. In other words, the QCISD method that is the second best ab initio method in the evaluation of barrier heights is strongly outperformed by the BB1K method. Even in comparison to QCISD(T) calculations, the BB1K method has a slightly lower mean energy error. A year after its proposal, this method was stated to be the most broadly accurate method for radical hydrogen abstraction, hydrogen transfer, heavy atom transfer, unimolecular, association, and even nucleophilic substitution reactions.[18] Also the MPWB1K method is the second best HMDFT one in the barrier height calculations and even is stronger than BB1K in calculation of binding energy of weakly bonded complexes.[18] The augmented polarized valence double-ξ basis set, 6-31+G(d,p), and the semidiffuse and modified version of the G3Large basis set, MG3S,[13] are used as the recommended basis sets for the aforementioned HMDFT methods.

The B3LYP and MP2 as commonly used HDFT and ab initio methods are implemented in comparison to the BB1K and MPWB1K methods in order to emphasis on the progressive remarks of the newly developed methods. The BB1K/6-31+G(d,p) method is utilized to produce geometries, electronic energies, and the first- and second-derivative matrices along the proton-transfer reaction path.

The minimum energy path (MEP) is constructed with the intrinsic reaction coordinate (IRC) method in the mass-weighted Cartesian coordinates with a step size of 0.02 $(\text{amu})^{1/2}$ bohr for each channel of the reaction.[19]

In this study also, the BMC−CCSD multicoefficient correlation method[20] for single-point energy (SPE) calculations is implemented in order to evaluate electronics barrier heights and the thermochemical properties. These types of methods use a linear combination of ab initio methods to extrapolate the exact nonrelativistic Born−Oppenheimer solution of the Schrödinger equation. The BMC−CCSD also benefits from the two new 6-31B(d) and MG3 basis sets that are stated to be correlation balanced.[20] The BMC−CCSD multicoefficient correlation method, proposed recently in 2005, is especially the most powerful multicoefficient method to estimate the barrier height[20] as

TABLE 1: Values of the Coefficients of BMC−CCSD Method

	coefficients				
method	c_H	c_1	c_2	c_3	c_4
BMC-CCSD	1.06047423	1.09791	1.33574	0.90363	1.55622

$$E(\text{BMC−CCSD}) = E(\text{HF/6-31B(d)}) + c_H\Delta(\text{HF/MG3|6-31B(d)}) + c_1\Delta(\text{MP2|HF/6-31B(d)}) + c_2\Delta(\text{MP2|HF/MG3|6-31B(d)}) + c_3\Delta(\text{MP4(DQ)|MP2/6-31B(d)}) + c_4\Delta(\text{CCSD|MP4(DQ)/6-31B(d)}) + E_{SO} \quad (1)$$

in which the pipe notation ("|") means the energy differences between the two methods. The values of coefficients are tabulated in Table 1. E_{SO} is the spin−orbit stabilization energy. It is considered to be zero for the closed-shell molecules and even for the CH_2FCHF radical, but for OH radical it is taken to be −0.20 kcal/mol.

Finally, the SPE correction at the BB1K/MG3S level of theory as higher level calculations for the TS and selected points along the MEP has been implemented to refine the PES shape.

The BSSE is accounted for in order to derive more accurate interaction energies for the molecular superstructures. The BSSE results in unphysical attraction between the fragments of a complex molecule when finite basis sets are used to calculate the interaction energy. We applied the standard counterpoise (CP) correction,[21] which attempts to correct for energy lowering of each fragment by extending the basis set with the ghost orbitals of another fragment. The corrections are applied for some selected points along the MEP in which the SPE correction has been used at BB1K/MG3S in order to have more refinement on the PES shape.

For the radical species, i.e., the open-shell systems, the unrestricted wave functions are used in the calculations. In general, wave functions for the open-shell systems are not eigenfunctions of the S^2 operator, where S is the electron spin operator. In particular, the wave functions for doublets are contaminated by quartets and higher multiplets. The wave functions for the superstructures along the MEP in radical reactions often suffer from the so-called "spin contamination" effect. Here an analysis of spin contaminations is presented for different applied methods. The spin-projected Möller−Plesset method (PMP2), in which contributions of higher multiplicity states are subtracted, has been utilized in comparison to the more elaborated MPWB1K, BB1K, and the well-known B3LYP density functional theory methods.

All electronic structure calculations are performed with Gaussian 2003.[22]

II.B. Dynamics Calculations. *II.B.1. Rate Constant Calculations.* Classical transition state theory rate constant calculation is based on assumption of quasi-equilibrium between reactants and the TS located on the dividing surface at the saddle point region of the PES. It means that in this theory, the energy profile

is the only criterion to determine the location of the TS for calculation of rate constant. Due to this postulate, the transition state theory only provides an upper bound for the exact rate constant. From a dynamical point of view, an overestimation occurs as a result of overcounting of trajectories which cross over the dividing surface, which is known as the "recrossing effect."[23] The variational transition state theory (VTST) minimizes the error from the recrossing effect by varying the location of the TS on the generalized dividing surface.[23a,d] The generalized dividing surface is a hypersurface that intersects the MEP perpendicular to it. In canonical variational transition state theory (CVT), the quantized partition functions are evaluated in the canonical ensemble at any temperature on the generalized dividing surface along the MEP in order to obtain the least classical flow. Thus, the thermal rate constant can be written as follows:

$$k^{\mathrm{CVT}}(T) = \min k^{\mathrm{GT}}(T, s) = k^{\mathrm{GT}}(T, s^{\mathrm{CVT}}(T)) \qquad (2)$$

where s is reaction coordinate parameter, $s^{\mathrm{CVT}}(T)$ is a specific value of s at which CVT rate constant is calculated, $k^{\mathrm{GT}}(T, s)$ is the generalized transition state rate constant which is evaluated at the generalized dividing surface and is expressed as

$$k^{\mathrm{GT}}(T, s) = \frac{\delta}{\beta h}\frac{Q^{\mathrm{GT}}(T, s)}{\phi^{\mathrm{R}}(T)}\exp\{-\beta V_{\mathrm{MEP}}(s)\} \qquad (3)$$

where $V_{\mathrm{MEP}}(s)$ is the classical potential energy along the MEP with its zero of energy on the reactants. Q^{GT} is the canonical partition function of the generalized TS with its local zero of energy on $V_{\mathrm{MEP}}(s)$, Φ^{R} is the reactant partition function per unit volume, h is Plank's constant, $\beta = (1/k_{\mathrm{B}}T)$, and δ is the symmetry factor that corresponds to the number of degenerated reaction paths that can also be evaluated as the ratio of the reactant rotational symmetry numbers to that of the TS. In the dual-level direct dynamics, electronic structure information is obtained from two levels of theory, in which the second higher level method is performed at the selected point along the MEP for improvement.[24] Here, the dual-level direct dynamics with the interpolated single-point energy method[25] (VTST−SPE) was used.

II.B.2. Tunneling Effects. The quantum effect on the motion along the reaction coordinate and its coupling to other degrees of freedom are included in the dynamics calculations by multiplying the CVT rate constant by a temperature-dependent transmission coefficient

$$k^{\mathrm{CVT}/Y}(T) = \kappa^{Y}(T)k^{\mathrm{CVT}}(T) \qquad (4)$$

Y indicates the correction method used for calculation of the transmission coefficient that can be obtained by different tunneling correction methods. The minimum energy path semiclassical adiabatic ground state (MEPSAG) method is appropriate if the principal tunneling path is along the reaction coordinate degree of freedom on the MEP. This approach is also known as the zero-curvature tunneling (ZCT) correction method.[23d] The small-curvature tunneling (SCT)[23d] transmission coefficients, that includes the reaction path curvature effect on the transmission probability, are based on the centrifugal-dominant small-curvature semiclassical adiabatic ground-state (CD-SCSAG) approximation.[23d] In particular, the transmission probability for energy E is given by

$$P(E) = \frac{1}{\{1 + \mathrm{e}^{-2\theta(E)}\}} \qquad (5)$$

where $\theta(E)$ is the imaginary action integral evaluated along the reaction coordinate, which is given by

$$\theta(E) = \frac{1}{\hbar}\int_{S_{\mathrm{i}}}^{S_{\mathrm{r}}}\sqrt{2\mu_{\mathrm{eff}}\,|E - V_{\mathrm{a}}^{\mathrm{G}}(s)|}\,\mathrm{d}s \qquad (6)$$

where the integration limits s_{i} and s_{r} are the reaction coordinate classical turning points. The reaction path curvature of the transverse modes effect on the tunneling probability is included in the effective reduced mass μ_{eff}. Renormalization of μ_{eff} is interpreted as a corner-cutting effect, which makes the barrier and resulted tunneling path thinner.

II.B.3. Hindered Rotors. All vibrational modes are treated as harmonic oscillators, except one or two of them depends on the reaction channels. Anharmonicity in the form of the hindered rotor treatment is considered for the lowest vibrational modes which correspond to internal rotations with torsional barriers comparable to *RT*. The vibrational partition functions of these modes are replaced by the hindered rotor partition function (Q^{HR}). Here, the method of "full approximation" is used to obtain Q^{HR}, in such a way that free rotor (Q^{FR}) in the limit of $kT \gg W$ and vibrational partition functions (Q^{HO}) in the limit of $kT \ll \hbar$ is used.[26] In the temperature range between these two extreme limits, i.e., $\hbar\upsilon \ll k \ll W$, the partition function is defined as

$$Q^{\mathrm{I}} = \frac{kT}{\hbar}\sum_{j=1}^{P}\frac{\mathrm{e}^{-U_j/kT}}{\nu_j} \qquad (7)$$

The above expression is the high-temperature limit of the vibrational partition function, in which U_j is the height of each distinct potential minimum relative to the lowest one, P is number of distinct minima, and k, T, $\hbar$, and υ are well-known physical constants. The corrected partition function can be expressed as

$$Q^{\mathrm{HR}} = Q^{\mathrm{HO}}\tanh(Q^{\mathrm{FR}}/Q^{\mathrm{I}}) \qquad (8)$$

In the present study, transition state and canonical variational transition state rate constants with zero-curvature and SCT correction methods are calculated. For the SCT calculations, the effective reduced mass is obtained by the Lagrangian interpolation of six order. The Euler single-step integrator[27] with a step size of 0.0005 $(\mathrm{amu})^{1/2}$ bohr is used to follow the MEP. The generalized normal-mode analysis is performed for each 0.001 $(\mathrm{amu})^{1/2}$ bohr. The curvature components of the MEP are calculated by using a quadratic fit (a central finite difference method[23]) to obtain the derivative of the gradient with respect to the reaction coordinate. Two electronic states of OH radical are included in the calculation of its electronic partition function, with a 140 cm^{-1} splitting (= 0.4 kcal, twice E_{SO}) for the $^2\Pi$ ground state.

All calculations are performed with "POLYRATE" code provided by Truhlar's group.[28]

III. Results and Discussion

III.A. Electronic Structure Properties. Hydrogen abstraction reaction takes place on two different conformations of CH_2FCH_2F, namely, the gauche and anti, also via two different OH

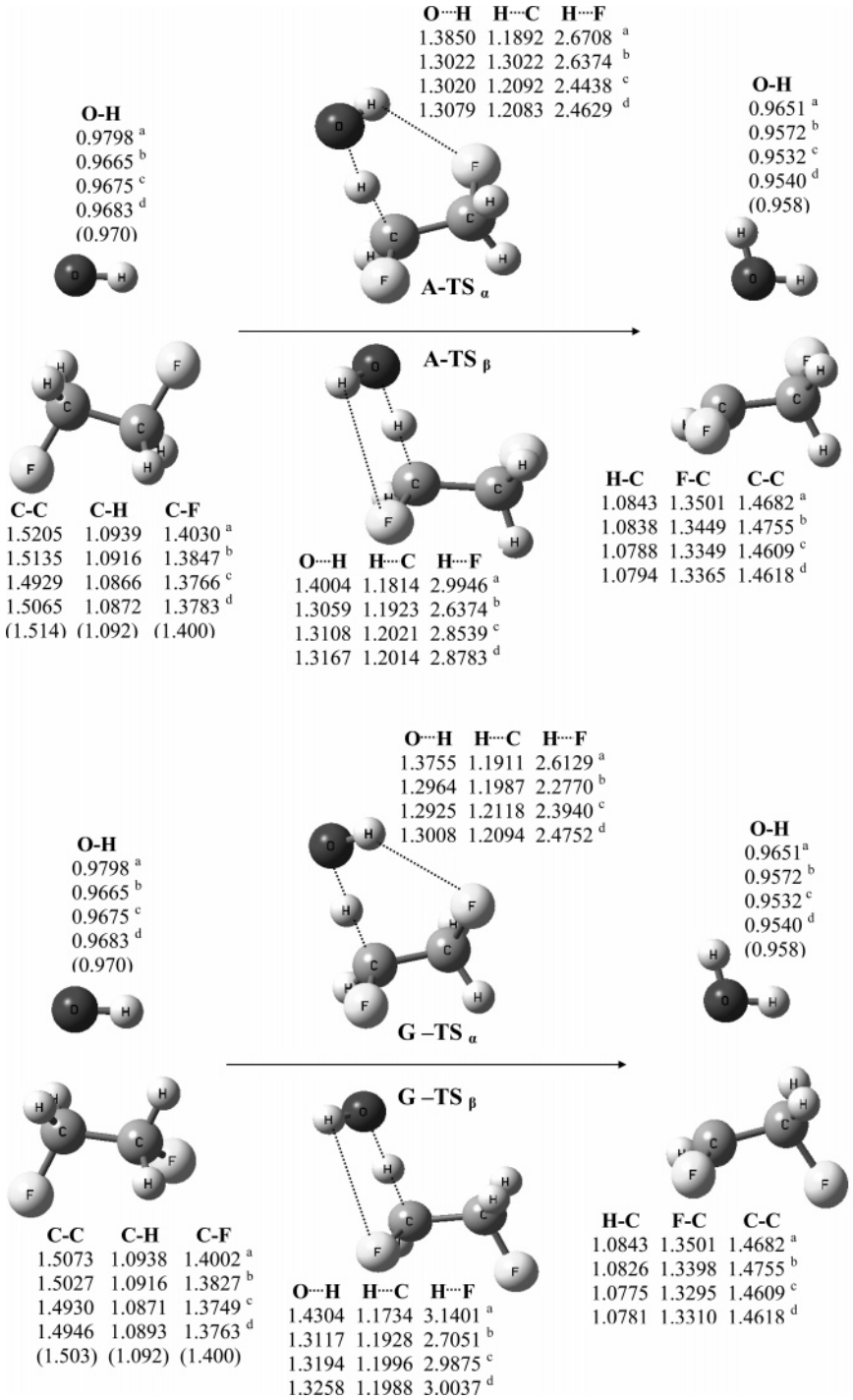

Figure 1. Equilibrium geometry of reactants, products, and transition states of different methods: (a) B3LYP, (b) MP2(Full), (c) MPWB1K, and (d) BB1K. Bond lengths are given in angstroms.

orientations. Here, we have labeled the channels of the reaction as follows:

channel 1:

$$CH_2FCH_2F\ (anti) + OH^{\bullet} \xrightarrow[A\text{-}TS_{\beta}]{A\text{-}TS_{\alpha}} CH_2FCHF^{\bullet}\ (anti) + H_2O$$

channel 2:

$$CH_2FCH_2F\ (gauche) + OH^{\bullet} \xrightarrow[G\text{-}TS_{\beta}]{G\text{-}TS_{\alpha}} CH_2FCHF^{\bullet}\ (gauche) + H_2O$$

Reactants, products, and transitions state species are depicted in Figure 1. The calculated values are in good agreement with experimental geometric data.[29] For the OH radical the best result is obtained by using the BB1K method. The OH orientation is the result of long-range intramolecular interactions. The BB1K and MPWB1K methods are able to produce more accurate long-range interaction energies and distances. The H···F distance provides indirect evident for nature of the interaction with comparing it to the van der Waals radius of hydrogen and fluorine atoms that are 1.3 and 1.2 Å, respectively. The H···F distance in the α and β structures is about 2.4 and 3.0 Å, respectively. The shorter H···F distances in the two α structures in comparison to the sum of the hydrogen and fluorine van der Waals radii, 2.5 Å, reflect their stronger hydrogen-bonding characteristics.

TABLE 2: Electronic Energy Changes of Reaction, Enthalpy Changes (at 298 K), and Barriers Height Calculated at Different Quantum Methods in kcal/mol for Channel 1[a]

			α structure		β structure	
method	ΔE_r	ΔH^0_r	E_b	E_b + ZPE	E_b	E_b + ZPE
MP2/6-311G(d,p)	−15.44	−15.99	7.37 (13.35)	6.00	8.11 (13.40)	6.46
MP2(Full)/6-311G(d,p)	−15.51	−16.07	7.22 (13.33)	5.85	7.95 (13.37)	6.31
PMP2/6-311G(d,p)	−15.58	−16.13	5.23 (11.32)	3.86	5.99 (11.39)	4.34
PMP2(Full)/6-311G(d,p)	−15.65	−16.21	5.23 (11.32)	3.71	5.84 (11.38)	4.20
B3LYP/6-31+G(d,p)	−18.46	−18.98	−0.30 (0.34)	−1.41	0.11 (0.68)	−1.03
MPWB1K/6-31+G(d,p)	−14.18	−14.71	3.98 (4.66)	2.41	4.55 (5.23)	2.68
BB1K/6-31+G(d,p)	−14.32	−14.85	4.42 (5.09)	2.88	4.91 (5.58)	3.09
BMC-CCSD//MP2(Full)/6-311G(d,p)[b]	−18.59	−19.15	2.89 (5.25)	1.52	3.57 (5.71)	1.93
BMC-CCSD//MPWB1K/6-31+G(d,p)	−18.59	−19.12	2.70 (4.94)	1.13	3.41 (5.46)	1.54
BMC-CCSD//BB1K/6-31+G(d,p)	−18.59	−19.12	2.76 (4.97)	1.22	3.68 (5.50)	1.66
BB1K/MG3S//BB1K/6-31+G(d,p)	−16.07	−16.60	3.93 (4.60)	2.39	4.48 (5.03)	2.66

[a] BSSE-corrected values are given in parentheses. ZPE stands for the zero-point energy corrections. [b] A//B sign means single-point calculation in A's level of theory based on the lower level geometry and frequency calculation of the B's method.

TABLE 3: Same as Table 2 for Channel 2

			α structure		β structure	
method	ΔE_r	ΔH^0_r	E_b	E_b + ZPE	E_b	E_b + ZPE
MP2/6-311G(d,p)	−16.84	−17.10	6.55 (12.54)	5.24	7.46 (12.54)	5.89
MP2(Full)/6-311G(d,p)	−16.90	−17.17	6.39 (12.52)	5.09	7.32 (12.53)	5.74
PMP2/6-311G(d,p)	−17.08	−17.34	4.40 (10.51)	3.09	5.34 (10.54)	3.77
PMP2(Full)/6-311G(d,p)	−17.15	−17.42	4.26 (10.51)	2.96	5.22 (12.52)	3.64
B3LYP/6-31+G(d,p)	−17.80	−18.75	−0.84 (−0.2 0)	−1.92	−0.84 (−0.30)	−1.69
MPWB1K/6-31+G(d,p)	−15.80	−16.08	3.33 (4.08)	1.78	3.73 (4.33)	1.91
BB1K/6-31+G(d,p)	−15.98	−16.25	3.79 (4.54)	2.29	4.07 (4.66)	2.31
BMC-CCSD//MP2(Full)/6-311G(d,p)[a]	−20.10	−20.37	2.36 (4.70)	1.06	2.94 (4.87)	1.36
BMC-CCSD//MPWB1K/6-31+G(d,p)	−20.38	−20.65	2.15 (4.41)	0.60	2.73 (4.76)	0.91
BMC-CCSD//BB1K/6-31+G(d,p)	−20.39	−20.66	2.24 (4.42)	0.74	2.80 (4.81)	1.04
BB1K/MG3S//BB1K/6-31+G(d,p)	−16.07	−16.34	3.55 (4.21)	2.05	3.89 (4.48)	2.13

[a] A//B sign means single-point calculation in A's level of theory based on the lower level geometry and frequency calculation of the B's method.

TABLE 4: The $\langle S^2 \rangle$ Value for Reactants, Products, and TS Structures of Different Methods

	chemical species						
method	$OH^\bullet$	A-TS_α	A-TS_β	G-TS_α	G-TS_β	$CH_2FCHF^\bullet$ (gauche)	$CH_2FCHF^\bullet$ (anti)
MP2/6-311G(d,p)	0.7548	0.7782	0.7779	0.7782	0.7780	0.7609	0.7598
B3LYP/6-31+G(d,p)	0.7524	0.7562	0.7562	0.7562	0.7562	0.7536	0.7536
MWPB1K/6-31+G(d,p)	0.7528	0.7607	0.7607	0.7607	0.7609	0.7540	0.7536
BB1K/6-31+G(d,p)	0.7527	0.7603	0.7602	0.7602	0.7604	0.7539	0.7536
BB1K/MG3S	0.7529	0.7606	0.7606	0.7606	0.7608	0.7541	0.7538

Electronic energy changes, enthalpy changes, and the classical barrier heights along its zero-point energy (ZPE) and BSSE-corrected values are tabulated in Tables 2 and 3 for the channels 1 and 2 of the reaction, respectively. At a glance it can be inferred that MP2 overestimates the classical barrier about twice higher than those of MPWB1K and BB1K. Also, BSSE is about 6 kcal/mol for MP2, whereas it is smaller than 1 kcal/mol for the HDFT methods. The slower trend in convergence of the energy values with basis set size for the MP2 method in comparison to the HDFT methods can be understood. The B3LYP produces completely incorrect barrier heights, but in contrast, produces more accurate values for the reaction energy and enthalpy changes, which are in a closer agreement with BMC−CCSD results. On the contrary, MPWB1K and BB1K produce inaccurate reaction electronic energy and enthalpy changes.

As presented in Tables 2 and 3, BSSE-corrected barrier heights for the last six quantum models are in very close agreement with each other, and the maximum discrepancy is smaller than 0.4 kcal/mol. For the BMC−CCSD quantum models, although BSSE was accounted by the applied adjusted coefficients, we have shown that BSSE correction has to be accounted for due to the existence of the intramolecular interaction in this system. The BSSE correction on BMC−CCSD barrier heights is evaluated in a nonstandard procedure. It is calculated for the E(HF/6-31B(d)) basic term in eq 1 in which correction terms resulted from basis set completeness and electron correlations were added in the form of the additive terms.

The frozen-core and full MP2 methods, which calculate correlation energy perturbatively for the valence electrons or all electrons, respectively, reproduce electronic energy with a negligible difference. In contrast, the spin-projected MP2 (PMP2) method reproduces the barrier heights in a closer agreement with the last six listed methods given in Tables 2 and 3. The PMP2 method estimates reaction barriers about 2 kcal/mol lower than MP2 due to the existence of large spin contamination error in the system understudy. For the doublet state of this system, deviation of the $\langle S^2 \rangle$ value from 0.7500 reflects the spin contaminations. As shown in Table 4, for the TS structures spin contaminations are larger than those of the reactant and product radicals. The spin contamination in the MP2 method is significantly larger than that of the HDFT methods. The B3LYP predicts the same values for different chemical species. Also, spin contamination in BB1K is lower than that of MWPB1K. Then it can be understood that the MEP

TABLE 5: Vibrational Frequencies of the Chemical Species in cm^{-1} and the Zero-Point Energy (ZPE) in kcal/mol[a]

species	frequencies (cm^{-1})										ZPE
CH_2FCH_2F	3208	3196	3140	3131	1520	1519	1478	1427	1332	1288	39.32
(gauche)	*3001*	*2995*	*2985*	*2958*	*1460*	*1460*	*1410*	*1377*	*1284*	*1244*	
	1170	1154	1137	930	902	502	327	148			
	1116	*1079*	*1076*	*896*	*865*	*500*	*327*	*147*			
CH_2FCH_2F	3227	3203	3153	3148	1555	1549	1487	1382	1323	1261	39.39
(anti)	*3001*	*2974*	*2985*	*2958*	*1490*	*1460*	*1454*	*1410*	*1377*	*1218*	
	1198	1131	1131	1113	826	469	281	118			
	1116	*1087*	*1079*	*1052*	*947*	*865*	*285*	*117*			
CH2FCHF•	3304	3218	3153	1517	1472	1389	1296	1261	1141	1013	30.30
(gauche)											
	936	603	459	307	125						
CH2FCHF•	3286	3164	3078	1528	1485	1351	1256	1228	1145	1127	30.11
(anti)											
	1004	584	480	292	54						
OH•	3856										5.51
	3735										
H_2O	4088	3962	1635								13.84
	3756	*3657*	*1595*								
A-TS_α	3885	3216	3189	3144	1538	1512	1434	1367	1350	1272	43.36
	1188	1171	1128	1110	890	846	608	460	310	268	
	187	143	111	1246 *i*							
A-TS_β	3889	3208	3189	3132	1534	1505	1440	1355	1319	1276	43.08
	1180	1159	1148	1114	904	810	709	472	286	172	
	144	114	72	1148 *i*							
G -TS_α	3882	3210	3183	3141	1515	1481	1448	1408	1308	1249	43.34
	1194	1158	1138	974	912	862	736	513	321	274	
	177	125	109	1274 *i*							
G -TS_β	3886	3223	3196	3153	1517	1489	1447	1370	1319	1290	43.08
	1195	1156	1132	933	922	889	738	467	328	168	
	148	90	79	1070 *i*							

[a] The italic values are experimental values (for OH and H_2O from ref 30 and for CH_2FCH_2F from ref 31).

calculated at the MP2 level has spin contamination errors in addition to the BSSE.

Due to large variation in the BSSE and spin contamination errors from TS to reactant and product regions, these two errors affect the PES shape significantly regardless of their effect on the barrier heights. On the basis of the analyses presented above, we chose the BB1K/MG3S//BB1K/6-31+G(d,p) quantum model for the direct dynamics calculations in which the MEP is calculated at the lower lever BB1K/6-31+G(d,p) method and SPE correction for some selected points are calculated at the higher level BB1K/MG3S method. The values of vibrational frequencies are presented in Table 5.

III.B. Dynamics Calculation. *III.B.1. Variational Effects.* An uncommon variational effect appears from the detailed analysis of the reaction under study. We have presented this analysis for channel 2-α for which the largest tunneling effect is detected. As depicted in Figure 2, channel 2α has a very smooth PES in the reactant region and low barrier height. The same plots are presented in the Supporting Information for the other channels. The intramolecular interaction which exists in the system somewhat compensates for the electronic energy lowering at the reactant side and results in a more smooth PES. Also, the loose structure located at the saddle point causes a remarkable decrease in the ZPE. The plots of normal-modes frequency changes demonstrate significant variations of one vibrational mode, Figure 3. We previously reported this U-shaped curve as a typical behavior for the H abstraction reactions.[5] The mentioned mode is an orthogonal mode to the reaction coordinate and transmutes from the C−H stretching vibration in the reactant molecule to symmetric O−H stretching vibration in the product. For the channel 2-α, the frequency of this mode reaches to 1515 cm^{-1} at the saddle point position and remains unchanged, $-0.2 < s < 0.11$ $(amu)^{1/2}$ bohr, in a small region around it. The same trend is observed for the other channels which are presented in the Supporting Information. For this channel changes of TST and CVT rate constants, variational effects, and bottleneck properties with temperature are given in Table 6. At low temperatures, the bottleneck of the reaction is located at −0.2, which is exactly at the same location in which the mentioned vibrational mode has started to increase in magnitude, see Figure 3. This channel of reaction has shown minimum error raised from variational effect in rate constant calculation between the others. The variational effect deviates the CVT rate constant from the TST through a factor of 11.1, 12.4, and 8.3 for channels 1-α, 1-*β*, and 2-*β*, respectively. As described here, ZPE for the loose TS structures

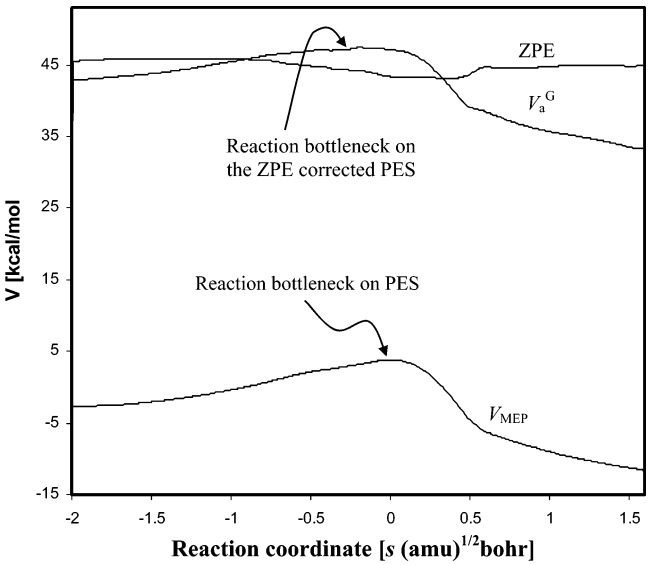

Figure 2. Variation of the minimum energy path (V_{MEP}), vibrationally adiabatic surface (V_a^G), and zero-point energy (ZPE) along the reaction coordinate for channel 2-α. The reaction coordinate is in mass-weighted Cartesian coordinate with its negative values in the reactant region.

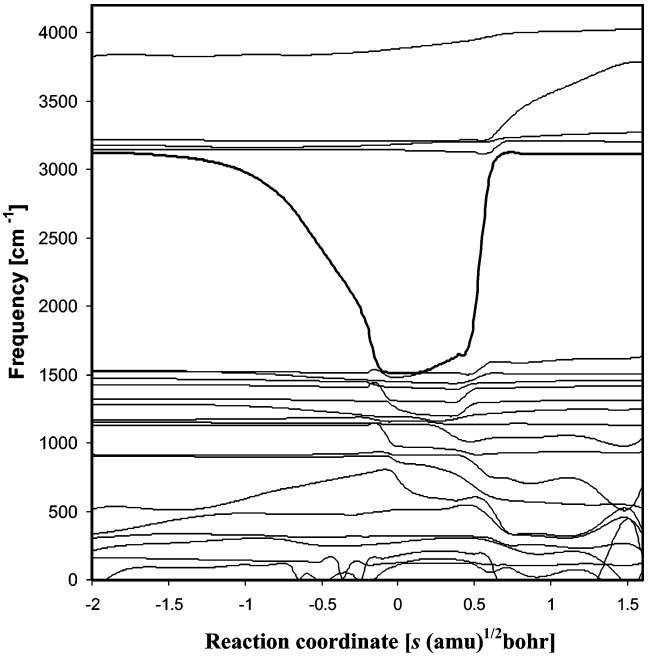

Figure 3. Changes of normal-mode frequencies along the reaction coordinate in channel 2-α. The reaction coordinate is in mass-weighted Cartesian coordinate with its negative values in the reactant region.

TABLE 6: Bottleneck Property of Channel 2-α and Its Change with Temperature[a]

T (K)	S	V_{MEP}	V_a^G	TST	VTST	TST/CVT
150.00	−0.196	3.425	47.655	1.25×10^{-16}	3.69×10^{-16}	3.39
250.00	−0.192	3.429	47.649	2.19×10^{-14}	1.20×10^{-14}	1.82
298.00	−0.189	3.433	47.643	4.67×10^{-14}	2.97×10^{-14}	1.57
375.00	−0.179	3.448	47.625	1.14×10^{-13}	8.34×10^{-14}	1.37
480.00	−0.172	3.459	47.609	2.72×10^{-13}	2.21×10^{-13}	1.23
800.00	−0.158	3.484	47.576	1.44×10^{-12}	1.28×10^{-12}	1.12
1200.00	−0.152	3.496	47.568	5.13×10^{-12}	4.58×10^{-12}	1.12
2000.00	−0.150	3.500	47.565	2.37×10^{-11}	2.08×10^{-11}	1.14

[a] Variational effects in rate constant are evaluated as the ratio of TST to CVT.

are smaller than ZPE of reactants. Subsequently, vibrational energy levels for the perturbed modes, depicted in Figure 3, are more closely spaced than reactants and products structures. Considering the assigned harmonic approximation and existence of same gap in the quantized vibrational energy levels for each normal mode, the height of the thermal energy corrected barriers diminish with temperature. In addition, due to the low barrier heights in the reaction, exponential factors in eq 3 rapidly converge to 1 as temperature increases. Hence, the variational effect, which is resulted from shift of the bottleneck, decreases at high temperatures. Since the significant perturbation of one vibrational mode is the cause of the described variational effect, utilization of more elaborate methods in which the rate constant is calculated in the microcanonical ensemble to evaluate reaction bottleneck at any E over the threshold classical barrier is not necessary.

III.B.2. Hindered Rotor Correction. Hindered rotor correction is used for TS low vibrational modes that have frequency lower than 120 cm^{-1} in Table 5. For α channels one vibrational mode and for β channels two vibrational modes are considered as hindered rotors. Direct inspection of the mentioned modes shows similar characteristics for the first and second modes of each channel. The first mode corresponds to rotation along the C−C bond with two different distinct minima, and the second mode corresponds to rotation of the reactive O−H bond along the reactive C−H bond with one minimum. The effects of hindered rotor treatment are plotted in Figure 4.

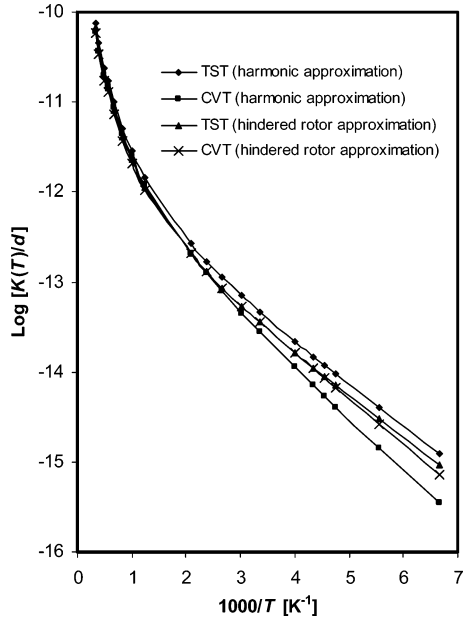

Figure 4. Arrhenius plot of rate constant calculated by TST and CVT methods for channel 2-α. Hindered rotor treatment of the normal mode with frequency of 109 cm^{-1} is compared with its harmonic approximation. The dimension of d is in the unit of cm^3 molecule^{-1} s^{-1}.

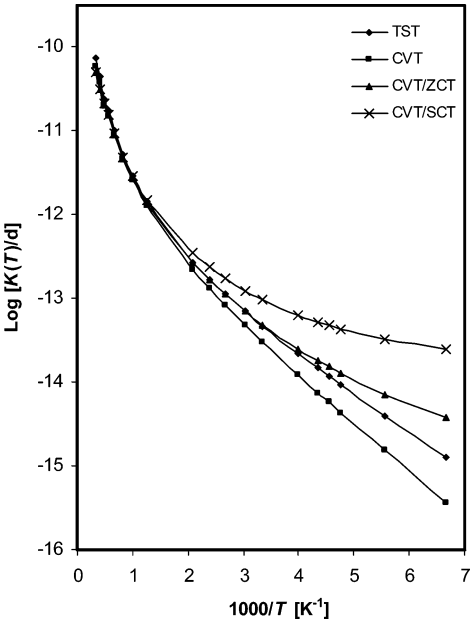

Figure 5. Arrhenius plot of rate constant calculated at TST, CVT, CVT/ZCT, and CVT/SCT methods for channel 2-α. The dimension of d is in the unit of cm^3 molecule^{-1} s^{-1}.

III.B.3. Tunneling Effects. As a result of the flat vibrational adiabatic potential surface, as discussed above, tunneling effects in this reaction are not high, but their contributions to the temperature dependency of the total rate constant are crucial. Arrhenius plots of the rate constant calculated at TST, CVT, CVT/ZCT, and CVT/SCT methods for channel 2-α are given in Figure 5. As shown, at the low-temperature limit tunneling enhances the reaction rate by 2 orders of magnitude. Also, from the large discrepancy between the ZCT and SCT correction methods, the importance of tunneling through multidimensional space, which is related to the concave side of the transverse modes perpendicular to the MEP, can be inferred. Similar plots

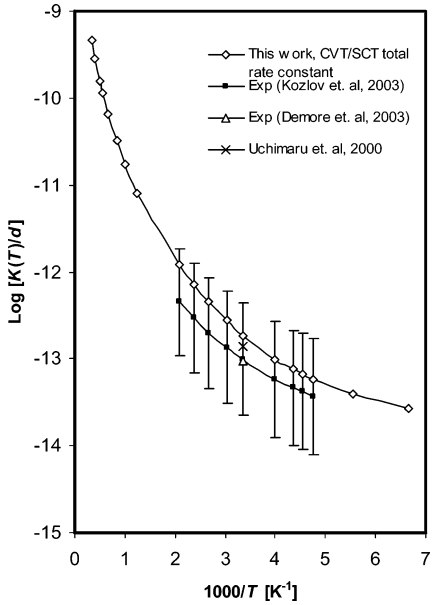

Figure 6. Arrhenius plot of total rate constant calculated at CVT/SCT as the most accurate method in comparison to experimental data. Error bars of 5% for Kozlov[9] data have been considered. Reported data of theoretical work of Uchimaru et. al[6] is included in which crude tunneling methods, Wigner's method, along with TST calculation has been used. Their reported data is based on MP2/6-311G(d,p) geometry and frequency calculation with SPE barrier height correction at MP2(full)/6-311G(3d,2p) as a quantum model build. The dimension of d is in the unit of cm^3 $molecule^{-1}$ s^{-1}.

are presented for the other channels of the reaction in the Supporting Information. For the other channels, the tunneling corrections are smaller and have the same order of magnitude of the reported variational effects.

III.B.4. Total Rate Constant. Contribution of both anti and gauche conformers of reactant molecules, as in the definition of channels 1 and 2 of the reaction presented, are taken into account by a Boltzmann weighting factor with $\Delta E = 0.61$ kcal/mol. Degeneracy of the reactive path is four in all channels except channel 2-α that has a path degeneracy of two. Path degeneracy can be obtained by the ratio of reactant symmetric numbers or intuitively by looking into the TS structure and counting the number of paths by which the OH radical approaches and reacts. On the basis of the presented quantum and dynamics models, the calculated total rate constant is in good agreement with experimental data, shown in Figure 6. In the low-temperature range, reaction occurs dominantly via channel 2-α.

IV. Summary

(1) The accurate rate constant of the reaction was obtained by canonical variational theory with the SCT correction method, consistent with experimental data over a wide temperature range, in which a dual-level direct density functional theory dynamics as the VTST−ISPE scheme was used. On the basis of our calculation, the temperature dependency of the total rate constant is obtained as follows:

$$k(T) = 5.4\times10^{-13}(T/298)^{3.13}\exp\{-322/T\}\ \mathrm{cm^3\ molecule^{-1}\ s^{-1}}$$

(2) An uncommon variation effects is detected as a result of the flat PES in this case. Our analysis shows that the variational effect is mainly due to the bottleneck change of the reactive channel resulted from the ZPE. More elaborated methods such as ICVT and μVT optimize the bottleneck for any E over the barrier in order to minimize the classical flow. Owing to the fact that change of the ZPE itself is mainly resulted from variation of only one vibrational mode, therefore, utilization of the more elaborated methods for the reaction is not necessary. The ICVT rate constant for channel 2-β is given in the Supporting Information.

(3) In general, errors coming from tunneling corrections and electronic structure calculation of barrier height may compensate each other in the rate constant calculation. Therefore, decision on possibility of error cancellation always remains obscure until the rate constant is compared with the experimental value for a large temperature range. In this study the utilized HMDFT methods are used to minimize the errors raised from spin contaminations and BSSE.

Acknowledgment. We thank Professor Donald G. Truhlar for providing the POLYRATE program. The financial support of the Iranian National Science Foundation and research council of the Sharif University of Technology are appreciated.

Supporting Information Available: Variation of the minimum energy path (V_{MEP}), vibrationally adiabatic surface (V_a^G), and zero-point energy (ZPE) along the reaction coordinate for different channels of the reaction (Figure S1), changes of normal-mode frequencies in the different channels, as same graphs as Figure 3 (Figure S2), results of the anharmonicity correction and tunneling corrections in rate constant calculation for the channels (Figures S3 and S4), and the ICVT rate constant for channel 2-α in comparison to the calculated rate constants (Table S1). This material is available free of charge via the Internet at http://pubs.acs.org.

References and Notes

(1) Tuck, R.; Plumb, A.; Condon, E. *Geophys. Res. Lett.* **1990**, *17*, 313.
(2) Manzer, L. *Science.* **1990**, *249*, 31.
(3) Atkinson, R. *Chem. Rev*. **1986**, *86*, 69.
(4) Good, A. D.; Francisco, S. *J. Chem. Rev.* **2003**, *103*, 4999.
(5) Taghikhani, M.; Parsafar, G. A.; Sabziyan, H. *J. Phys. Chem. A* **2005**, *109*, 8158.
(6) Chandra, A.; Uchimaru, T.; Sugie, M. *J. Comput. Chem.* **2000**, *21*, 1305.
(7) Kwok, E. S. C.; Atkinson, R. *Atmos. Environ.* **1995**, *29*, 1685.
(8) Hsu, K. J.; DeMore, W. B. *J. Phys. Chem.* **1995**, *99*, 11141.
(9) Kozlov, S. N.; Orkin, V. L; Kurylo, M. J. *J. Phys. Chem. A* **2003**, *107*, 2239.
(10) Wilson, E. W; Jacoby, A. M.; Jkukta, S.; Gilbert, S. J.; DeMore, W. B. *J. Phys. Chem. A* **2003**, *107*, 9357.
(11) Zhao, Y.; Schultz, N. E.; Truhlar, D. G. *J. Chem. Theory Comput.* **2006**, *2*, 364.
(12) Zhao, Y.; Truhlar, D. G. *J. Phys. Chem. A* **2005**, *109*, 5656.
(13) Zhao, Y.; Truhlar, D. G. *J. Phys. Chem. A* **2004**, *108*, 6908.
(14) Zhao, Y.; Lynch, B. J.; Truhlar, D. G. *J. Phys. Chem. A* **2004**, *108*, 2715.
(15) Becke, A. D. *Phys. Rev. A* **1988**, *38*, 3098.
(16) Becke, A. D. *J. Chem. Phys*. **1996**, *104*, 1040.
(17) Both the MPWB1K and BB1K methods benefited from the one-parameter hybrid Fock−Kohn−Sham operator in which different percentages of Hartree−Fock exchange operator are used. This is written as follows:

$$\mathbf{F} = \mathbf{F}^{H} + X\mathbf{F}^{HFE} + (1 - X)(\mathbf{F}^{SE} + \mathbf{F}^{GCE}) + \mathbf{F}^{Cor}$$

where $\mathbf{F}^{H}$ is the Hartree operator, $\mathbf{F}^{HFE}$ is the Hartree−Fock exchange operator, $\mathbf{F}^{SE}$ is the Dirac−Slater local density functional for exchange, $\mathbf{F}^{GCE}$ is the gradient correction for the exchange functional, and $\mathbf{F}^{Cor}$ is the total correlation functional including both local and gradient-corrected parts; also a kinetics energy density term is included. In the BB1K method, the Becke88 exchange functional for $\mathbf{F}^{GCE}$ and Becke95 correlation functional for $\mathbf{F}^{Cor}$ are used. In a similar way, in the MPWB1K method the same correlation functional has been used, and the difference is utilizing the modified Perdew−Wang functional as an exchange functional. X is the fraction of Hartree−Fock exchange operator and is 0.44 and 0.42 for

MPWB1K and BB1K, respectively. BB1K and MPWB1K can be implemented in GAUSSIAN 03 by using the b1b95 IOp(3/76=0580004200) and mpwb95/6-31+G(d,p) IOp(3/76=0560004400) keywords, respectively. Additional information on the implementation of these methods can be found on the Internet at http://comp.chem.umn.edu/info/DFT.htm.

(18) Zhao, Y.; Gonzales-Garcia, N.; Truhlar, D. G. *J. Phys. Chem. A* **2005**, *109*, 2012.

(19) (a) Gonzalez, C.; Schlegel, H. B. *J. Chem. Phys.* **1989**, *90*, 2154. (b) Gonzalez, C.; Schlegel, H. B. *J. Phys. Chem.* **1990**, *94*, 5523.

(20) Lynch, B. J.; Zhao, Y.; Truhlar, D. G. *J. Phys. Chem. A* **2005**, *109*, 1643.

(21) (a) Jansen, H. B.; Ross, P. *Chem. Phys. Lett.* **1969**, *3*, 140. (b) Boys, S. F.; Bernardi, F. *Chem. Phys.* **1970**, *232*, 299. (c) Tao, F.-M. *Int. Rev. Phys. Chem.* **2001**, *20*, 617.

(22) Frisch, M. J.; Trucks, G. W.; Schlegel, H. B.; Scuseria, G. E.; Robb, M. A.; Cheeseman, J. R.; Montgomery, J. A., Jr.; Vreven, T.; Kudin, K. N.; Burant, J. C.; Millam, J. M.; Iyengar, S. S.; Tomasi, J.; Barone, V.; Mennucci, B.; Cossi, M.; Scalmani, G.; Rega, N.; Petersson, G. A.; Nakatsuji, H.; Hada, M.; Ehara, M.; Toyota, K.; Fukuda, R.; Hasegawa, J.;Ishida, M.; Nakajima, T.; Honda, Y.; Kitao, O.; Nakai, H.; Klene, M.; Li, X.; Knox, J. E.; Hratchian, H. P.; Cross, J. B.; Bakken, V.; Adamo, C.; Jaramillo, J.; Gomperts, R.; Stratmann, R. E.; Yazyev, O.; Austin, A. J.; Cammi, R.; Pomelli, C.; Ochterski, J. W.; Ayala, P. Y.; Morokuma, K.; Voth, G. A.; Salvador, P.; Dannenberg, J. J.; Zakrzewski, V. G.; Dapprich, S.; Daniels, A. D.; Strain, M. C.; Farkas, O.; Malick, D. K.; Rabuck, A. D.; Raghavachari, K.; Foresman, J. B.; Ortiz, J. V.; Cui, Q.; Baboul, A. G.; Clifford, S.; Cioslowski, J.; Stefanov, B. B.; Liu, G.; Liashenko, A.; Piskorz, P.; Komaromi, I.; Martin, R. L.; Fox, D. J.; Keith, T.; Al-Laham, M. A.; Peng, C. Y.; Nanayakkara, A.; Challacombe, M.; Gill, P. M. W.; Johnson, B.; Chen, W.; Wong, M. W.; Gonzalez, C.; Pople, J. A. *Gaussian 03*, revision C.02; Gaussian, Inc.: Wallingford, CT, 2004.

(23) (a) Truhlar, D. G.; Garrett, B. C. *Annu. Rev. Phys. Chem.* **1984**, *35*, 159. (b) Truong, T. N. *J. Chem. Phys.* **1994**, *100*, 8014. (c) Truhlar, D. G.; Fast, P. L. *J. Chem. Phys.* **1998**, *109*, 3721. (d) Truhlar, D. G.; Isaacson, A. D.; Garrett, B. C. In *Theory of Chemical Reaction Dynamics*; Baer, M., Ed.; CRC Press: Boca Raton FL, 1985; Vol. 4, Chapter 2.

(24) Truhlar, D. G. Direct Dynamics Method for the Calculation of Reaction Rates. In *The Reaction Path in Chemistry: Current Approaches and Perspectives*; Heidrich, D., Ed.; Kluwer: Dordrecht, The Netherlands, 1995; p 229.

(25) Chuang, Y-Y.; Truhlar, D. G. *J. Chem. Phys.* **1999**, *103*, 1140.

(26) Chuang, Y-Y.; Truhlar, D. G. *J. Chem. Phys.* **2000**, *112*, 1221.

(27) Garrett, B. C.; Truhlar, D. G. *J. Chem. Phys.* **1979**, *83*, 3058.

(28) Jose, C. C.; Chuang, Y-Y.; Fast, P. L.; Villa, J.; Hu, W-P.; Liu, Y-P.; Lynch, G. C.; Nguyen, K. A.; Jackels, C. F.; Melissas, V. S.; Lynch, B. J.; Rossi, I.; Coitino, E.; Fernandez-Ramos, A.; Pu, J.; Albu, T. V. POLYRATE, version 9.1. Department of Chemistry and Supercomputer Institute, University of Minnesota, Minneapolis, Minnesota, 2002.

(29) NIST Standard Reference Database Number 69. http://webbook.nist.gov/chemistry/ (released March, 2003).

(30) Chase, M. W., Jr. *NIST−JANAF Themochemical Tables*, 4th ed. *J. Phys. Chem. Ref. Data* **1998**, Monograph 9.

(31) McNaughton, D.; Evans, C. *J. Phys. Chem.* **1996**, *100*, 8660.